IDENTIFYING THE STRUCTURAL ARCHITECTURE OF THE HUMAN INFERIOR PARIETAL LOBULE USING DIFFUSION MRI

R F Tungaraza[1,4], J J Howbert[5], S H Mehta[1,2,4], D R Haynor[1], L G Shapiro[3,4], and T J Grabowski[1,4]

Departments of [1]Radiology, [2]Psychology, [3]Computer Science and Engineering,
and [4]the Integrated Brain Imaging Center, University of Washington, and [5]Insilicos LLC, Seattle

ABSTRACT

Using a data-driven analysis of diffusion MRI called connectivity based cortical parcellation, we were able to segment the human inferior parietal lobule into spatially contiguous regions that closely match the human cytoarchitectonic atlas. This supports the cortical field hypothesis in that connectivity profiles appear to define the same field boundaries as histologic features. Here we present an approach and evaluation method for connectivity-based cortical parcellation.

Index Terms— diffusion MRI, bipartite matching, tractography, ensemble clustering, cytoarchitecture, inferior parietal lobule, cortical fields, parcellation

1. INTRODUCTION

The Cortical Field Hypothesis (CFH) is the notion that the human cerebral cortex is a mosaic of units, each occupying a contiguous territory of the cortex [1], as approximated by the classic cytoarchitectonic parcellations of Brodmann, von Economo, and others. A cortical field is posited to have a distinct cytoarchitecture (microstructural features of laminar thickness, cell size, packing density, etc [2]), myeloarchitecture (differential density of myelinated fibres in cortical layers [3]), neurotransmitter receptor complement [3]), and, in more recent thinking [3] pattern of connectivity to other cortical fields. The last characteristic in particular is an hypothesis with limited empirical data in human material. Also intrinsic to the CFH is the idea that each field has functional unity [1].

A number of studies have begun to exploit diffusion-weighted MRI in order to segment gray matter structures including thalamus and cerebral cortex into parcels with distinct connectivity profiles, an approach known as connectivity-based cortical parcellation (CBCP) [2]. CBCP rests on the premise that spatially adjacent voxels with similar long-range structural connectivity patterns can be clustered into spatially contiguous regions that resemble cortical fields. The notion that such connectivity parcels may be coextensive with fields defined by cytoarchitecture or myeloarchitecture is an intriguing one that appeals to the notion of functional unity and that may lead to a tractable approach to segmenting cortical fields in vivo.

In this project, we used CBCP to segment the human Inferior Parietal Lobule (IPL) in each hemisphere. We sought to quantify the extent to which the CBCP-driven parcellation resembled the human cytoarchitectonic map, using the standard probabilistic cytoarchitectonic atlas developed by the Jülich group from 10 postmortem human brain specimens [4]. A close resemblance would lend strong support to the CFH, by providing evidence that the cytoarchitectonically defined fields have distinct patterns of connectivity and that these characteristics define the same field borders. For our purpose we used a CBCP approach that did not use voxel position as a feature, and asked the question of whether a pattern of contiguous discrete patches would emerge from parcellation based on connectivity profiles alone.

The Jülich atlas is a data-driven, observer-independent segmentation of post-mortem tissue and represents the best available cytoarchitectonic standard. Data from the ten normal brains mentioned above, are represented as probability clouds in a standard anatomical space (MNI space). The probability clouds include segmentations of the right and left IPL, each into seven cytoarchitectonic fields (Figure 4).

In Section 2, we give a detailed description of our implementation of CBCP, and Section 3 presents our approach to validation. Section 4 presents our results and discussion, and Section 5 is our conclusion.

2. METHODOLOGY

2.1. Tractogram creation

The CBCP technique is based on the use of diffusion-weighted MRI (DWI) to estimate the most likely pathway of water diffusion, and infer the directional structure of white matter [2]. Some of these pathways have been shown to correspond to known axonal fiber tracts [3, 2]. Our data consisted of DWI (64 unique directions and b-value of 1000 mm/s^2), 2 mm isotropic resolution in 19 healthy-control subjects, using a Siemens Trio 3T scanner. After preprocessing the individual DWI volumes to remove noise and eddy current distortions using FSL [5], we extracted a 2 mm thick cortico-subcortical shell using FreeSurfer [6] in each subject's T1-weighted image. We mapped these segmentations

into the subject's DWI space and used the voxels along that ribbon to define both the target regions and seed voxels for probabilistic tractography. There were 91 possible target regions including all the Destrieux atlas [7] regions ipsilateral to the seed voxel, and the following subcortical regions: thalamus, caudate, putamen, pallidum, hippocampus, amygdala, accumbens area, cerebellum, and brain-stem. The seed voxels were the cortico-subcortical voxels of the angular gyrus, supramarginal gyrus, and Jensen sulcus of the Destrieux atlas regions. We performed probabilistic tractography from each seed voxel to each target region using MRtrix [8], rejecting all fiber tracks that started and ended in the same region. The product of this step was a two-dimensional matrix, in which each row represents the connectivity profile, or tractogram, of a voxel in the seed region with the 91 target regions.

2.2. Tractogram preprocessing

We reduced the tractogram dimensions nonlinearly such that the transformed space had only three dimensions. This helped us to (1) remove noise due to errors in tractography, (2) minimize the effects of redundant/collinear features in our dataset, and (3) visualize the local and global structure of tractograms prior to performing the clustering. We empirically ascertained that the tractograms lay on a low-dimensional manifold by experimenting with both Principal Components Analysis (PCA) and t-Distributed Stochastic Neighborhood Embedding (t-SNE) (described and evaluated in [9]). t-SNE is a nonlinear dimension reduction and data visualization technique that has been shown to outperform a number of other well-known non-linear dimensionality reduction techniques when the data are reduced to 2 or 3 dimensions. Figure 1 depicts the results of t-SNE and PCA in one subject. A clustering into 7 groups is visually evident in the t-SNE results (left), but not with PCA (right).We observed similar results in 15 of the 18 other subjects.

2.3. Ensemble clustering

After dimension reduction, we used ensemble clustering, with fuzzy c-means as the base clustering method to segment each hemisphere's seed region (Section 2.1) into seven partitions.

Fuzzy c-means [10] is a variant of k-means clustering. The algorithms differ in the way they assign each data point to a cluster: k-means creates a hard partition of the data points (i.e. separates them into k-disjoint sets) while fuzzy c-means provides for each data-point the degree of membership it has to all k-cluster centroids. One of the drawbacks of iterative descent methods like fuzzy c-means is the sensitivity to initialization parameters, which can lead to different clustering results with multiple runs of the same data.

In order to minimize this problem we employed ensemble clustering, a technique that attempts to generate a consensus cluster assignment (labeling) of data points given multiple runs of the same clustering method (where each run has a different random starting point). We used the ensemble clustering method of Strehl and Ghosh [11] to run fuzzy c-means clustering 200 times on the 3D-Tractograms. Each run had a different random starting partition. We then gave the resulting 200 labelings to the ensembler in order to obtain a consensus clustering. We repeated this 20 times for each subject, in order to assess the stability of the clustering.

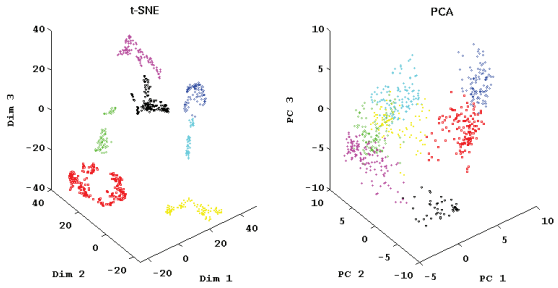


Fig. 1. Dimensionality reduction via t-SNE (left) versus PCA (right). The data points of the 3D-tractograms based on t-SNE depict both its local and global structure. The subsequent clustering into seven groups is visually evident (each color and marker represent members of one group). This is not the case for the 3D-tractograms based on PCA.

2.4. Projection of parcellation data onto the cortex

We projected the parcellations (i.e. the clusterings obtained in Section 2.3), which were computed along the cortico-subcortical ribbon, back onto the cortex. This was followed by mapping each subject's parcellation from diffusion MRI space to the MNI standard space. Lastly, we computed the center of gravity for each IPL sub-region in MNI space.

3. EVALUATION

3.1. Ensembler performance evaluation

To quantify the performance of the cluster ensembler we used maximum weight bipartite graph matching (MaWBM) [12] to compute a consistency score for each unique pair of consensus clusterings among the 20 generated for each subject. The complete bipartite graph comprised two sets of seven vertices, each set representing the seven IPL sub-regions of one of the two consensus clusterings in the pair. Each edge-weight in the graph corresponded to the amount of voxel overlap between two IPL sub-regions from the two consensus clusterings. The MaWBM finds a perfect matching between the two sets of vertices such that the sum of the edge-weights of that matching is maximal. After computing this score, we normalized it (i.e. divided the score generated by MaWBM by the total number of voxels in the overall IPL region). A score of 1

meant two IPL clusterings are exact matches, while a score of 0 meant no two clusters of the two IPL clusterings contained the same voxels. We then computed the mean and standard deviations of the normalized MaWBM scores for all the 190 possible pairs of consensus clusterings in each subject. This is the mean consistency score and its corresponding standard deviation. Both values gave us an indication of how consistently the ensembler was able to generate the same clustering in the same IPL.

3.2. Correspondence with cytoarchitectonic parcellations

To compare our IPL segmentation to the cytoarchitectonic atlas, we first identified the "most representative" clustering among the 20 consensus clusterings of each subjects IPL region. This was the clustering with the largest sum of MaWBM scores between itself and all the other 19 clusterings. Then we labeled each of its seven sub-regions with one of the seven cytoarchitectonic cluster labels. We assigned labels by constructing a complete bipartite graph with one vertex set based on the cytoarchitectonic sub-regions and the other vertex set based on the CBCP parcels in the same hemisphere. The weights of the edges in this graph were the Euclidean distances between the centers of gravity of each possible pair of sub-regions. We used minimum weight bipartite graph matching (MiWBM) [12] to find a perfect matching of these two sets of vertices such that the sum of the edge-weights was minimal. We used the resulting matching to label our IPL parcels. In order to quantify the degree of similarity between the CBCP IPL parcellations and the cytoarchitectonic atlas, we (1) computed the mean and standard deviations of the centers of gravity given all 19 centers of gravity of the same label along the same hemisphere and (2) computed the maximum probability map (MPM) for each hemisphere. A MPM is a map in which each voxel is assigned to the label to which it has the highest probability [13].

4. RESULTS AND DISCUSSION

Our approach to CBCP gave partitions of the IPL that were consistent in individual subjects. With the exception of two subjects' left hemispheres, all other mean consistency scores were above 0.87 and their corresponding standard deviations were less than 0.07 bilaterally when using ensemble clustering (See Figure 2). Similarly, the averages of the mean consistency scores were higher when we used ensemble clustering compared to when we did not use ensemble clustering, which underscores the need to repeat the clustering step of CBCP multiple times with different initialization points in order to ascertain that the results one gets are robust.

More strikingly, we also found that our CBCP approach segments the IPL, bilaterally, into sub-regions that closely resemble post-mortem data-driven cytoarchitectonic parcellations. In Figure 3, the mean centers of gravity of the CBCP

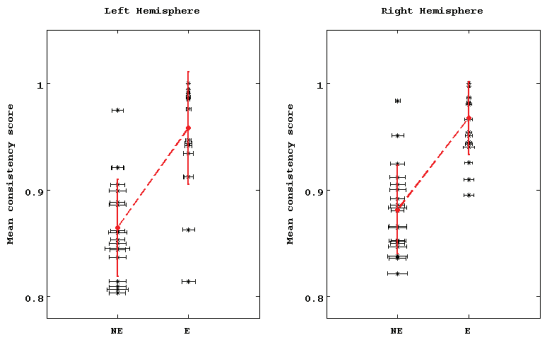


Fig. 2. Mean consistency scores across 19 subjects (black *) and corresponding standard deviations (horizontal bars, created by rotating the original vertical bars 90-degrees for visualization) obtained without using the ensembler (NE: the mean consistency score of 20 runs of fuzzy c-means with random initialization points) versus using the ensembler (E: the mean consistency scores were computed as described in Section 3.1) for both the left and right hemispheres IPL regions. The red dot in each column is the average mean consistency score across all 19 subjects while the red vertical bars are the corresponding standard deviations. The dotted line connecting the red dots highlights that the average mean consistency score for 'E' is higher than that of 'NE', indicating that formal supporting statistical information inherent in ensemble clustering tends to stabilize the parcellations.

sub-regions generally fall within the standard deviations of the mean centers of gravity of the cytoarchitectonic parcellations. There were a few exceptions, namely the PFm and PGp for the right IPL and the PFcm for the left IPL. Likewise, the MPMs for the CBCP sub-regions depicted in Figure 4 for the left hemisphere (right hemisphere not shown due to space contraints) show strong resemblance to the cytoarchitectonic parcellation except for the two rostral regions (PFcm and PFt). There are some possible methodological reasons for these discrepancies including: (1) We projected the parcellations of the cortico-subcortical ribbon onto the cortex, whereas in constrast the Jülich cytoarchitectonic parcellations were done on the cortex; (2) The data are from two different subject samples (ten postmortem brains ages 37-85 and 19 living healthy young adults), and there maybe between-group differences; (3) There are problems mapping postmortem data into standard space, though the Jülich methods attempt to minimize them.

We emphasize that we did not use the spatial locations of the voxels for our CBCP approach, yet the clusters that were obtained were contiguous rather than spatially mingled. This finding is consistent with the notion that connectivity profiles are a distinct defining feature of cortical fields.

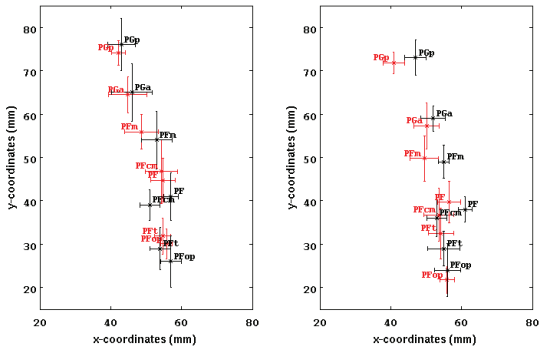


Fig. 3. Correspondence between the mean center of gravity of the cytoarchitectonic parcellations (in black) and the CBCP parcellations (in red) for the left hemisphere (left) and right hemisphere (right) in the X-Y plane (axial view; x- and y-coordinates are in absolute values). Error bars represent x- and y- standard deviations of the mean center of gravity.

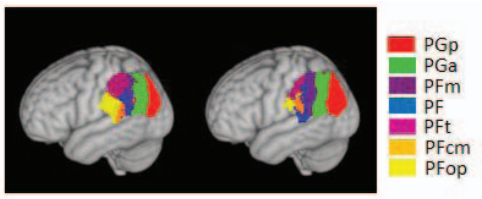


Fig. 4. MPMs of the CBCP parcellations (left) and cytoarchitectonic parcellations (right) for the left hemisphere.

5. CONCLUSION

Using a data-driven analysis of diffusion MRI we were able to segment the human inferior parietal lobule into spatially contiguous regions that closely match the best available human cytoarchitectonic data. This supports the cortical field hypothesis in the sense that connectivity profiles appear to define the same field boundaries as histologic features. If this same structure can be detected with analysis of diffusion MRI data, then a critical level of description of cortical neural systems will become accessible for in vivo human studies. Such data would be fundamentally useful to the study of human variation and brain function. These preliminary findings motivate refinement of the approach and justify more rigorous validation studies. Further work will be needed to establish whether parcels so identified have a neurophysiologic unity.

6. REFERENCES

[1] P. Roland and K. Zilles, "Structural divisions and functional fields in the human cerebral cortex.," *Brain research. Brain research reviews*, vol. 26, no. 2-3, pp. 87–105, May 1998.

[2] T. Behrens, J. Klein, S. Jbabdi, and H. Johansen-berg, "Connectivity-based parcellation of gray matter," in *Diffusion MRI: theory, methods, and applications*, Derek K Jones, Ed., chapter 24, pp. 409–424. Oxford University Press, Oxford, 1 edition, 2011.

[3] A Toga, P. Thompson, S. Mori, K. Amunts, and K. Zilles, "Towards multimodal atlases of the human brain.," *Nature reviews. Neuroscience*, vol. 7, no. 12, pp. 952–66, Dec. 2006.

[4] S. Caspers, S. Eickhoff, S. Geyer, F. Scheperjans, H. Mohlberg, K. Zilles, and K. Amunts, "The human inferior parietal lobule in stereotaxic space.," *Brain structure & function*, vol. 212, no. 6, pp. 481–95, Aug. 2008.

[5] S. Smith, M. Jenkinson, M. Woolrich, C. Beckmann, T. Behrens, H. Johansen-berg, P. Bannister, M. Luca, I. Drobnjak, D. Flitney, R. Niazy, J. Saunders, J. Vickers, Y. Zhang, N. Stefano, J. Brady, and P. Matthews, "Advances in functional and structural MR image analysis and implementation as FSL," *Neuroimage*, vol. 23, no. S1, pp. 208–219, 2004.

[6] A. Dale, B. Fischl, and M Sereno, "Cortical surface-based analysis I. segmentation and surface reconstruction," *NeuroImage*, vol. 9, no. 2, pp. 179–194, Feb. 1999.

[7] C. Destrieux, B. Fischl, A. Dale, and E. Halgren, "Automatic parcellation of human cortical gyri and sulci using standard anatomical nomenclature.," *NeuroImage*, vol. 53, no. 1, pp. 1–15, 2010.

[8] J-D. Tournier, F. Calamante, and A. Connelly, "Robust determination of the fibre orientation distribution in diffusion MRI : Non-negativity constrained super-resolved spherical deconvolution," *Brain Research*, vol. 35, pp. 1459 – 1472, 2007.

[9] L. Maaten and G. Hinton, "Visualizing data using t-SNE," *Journal of Machine Learning Research*, vol. 9, pp. 2579–2605, 2008.

[10] R. Nock and F. Nielsen, "On weighting clustering.," *IEEE TPAMI*, vol. 28, no. 8, pp. 1223–35, Aug. 2006.

[11] A. Strehl and J. Ghosh, "Cluster ensembles a knowledge reuse framework for combining partitionings," *AAAI*, 2002.

[12] R. Burkard, M. Dell'Amico, and S. Martello, *Assignment Problems*, SIAM, Philadelphia, 1 edition, 2009.

[13] S. Eickhoff, K. Stephan, H. Mohlberg, C. Grefkes, G. Fink, K. Amunts, and K. Zilles, "A new SPM toolbox for combining probabilistic cytoarchitectonic maps and functional imaging data.," *NeuroImage*, vol. 25, no. 4, pp. 1325–35, May 2005.